RSC Advances

PAPER

View Article Online
View Journal | View Issue

Open Access Article. Published on 28 September 2020. Downloaded on 11/29/2025 9:39:57 AM.
This article is licensed under a Creative Commons Attribution-NonCommercial 3.0 Unported Licence.

Check for updates

Cite this: *RSC Adv.*, 2020, **10**, 35646

Cooperation of Fe(II) and peroxymonosulfate for enhancement of sulfamethoxazole photodegradation: mechanism study and toxicity elimination†

Han Gong,[a] Wei Chu,*[b] He Gong,[c] Airu Huang,[a] Jingjun Lin[a] and Muting Yan *[a]

This study aims at systematically examining the potential of removing the emerging pollutant sulfamethoxazole (SMX) from aqueous solution under photo-assisted peroxymonosulfate (PMS) activation by Fe(II). The residual SMX was determined by HPLC analysis. The concentration of Fe(II) ([Fe(II)]) was monitored during SMX degradation. Fe(II) and PMS cooperated with each other for faster SMX photodegradation; a relatively lower or higher molar ratio between Fe(II) and PMS led to lower SMX removal efficiency due to the insufficient radicals or scavenging effect. A fixed reaction ratio of $[Fe(II)]_{\Delta}$: $[PMS]_0$ with 1.6 : 1 at the first 5 min was detected for reactions with $[Fe(II)]_0 \geq 0.5$ mM or $[PMS]_0 \leq 0.25$ mM. The pH level of around 6.0 was recommended for optimal SMX removal under the treatment process UVA + Fe(II) + PMS. Six transformation products were detected through UPLC/ESI-MS analysis, and four of the proposed intermediates were newly reported. Concentrations of the intermediates were proposed based on the isoxazole-ring balance and the Beer–Lambert law. Total Organic Carbon (TOC) reduction was mainly attributed to the loss of benzene ring, N–S cleavage, and isoxazole ring opening during SMX degradation. The contributions of reactive species $OH^{\bullet}$ and $SO_4^{\bullet-}$ were determined based on quench tests. The acute toxicity of SMX to the rotifers was eliminated after the proposed treatment, demonstrating that the process was effective for SMX treatment and safe to the environment.

Received 30th June 2020
Accepted 10th September 2020

DOI: 10.1039/d0ra05704e

rsc.li/rsc-advances

1. Introduction

Pharmaceuticals and personal care products, PPCPs, being detected in natural waters, have raised global concern for their potential environmental and health effects.[1] Sulfamethoxazole (SMX) is a pharmaceutical that is largely used for the treatment of bacterial infections such as urinary tract infections, bronchitis, and prostatitis. A previous study showed that SMX has low biodegradability and may result in direct or indirect toxicological effects on the environment and human health.[2] Especially, as an antibiotic, residues of SMX may pose a potential risk for developing antibiotic resistant bacteria.[3]

Common water/wastewater treatments processes cannot effectively remove antibiotics including SMX because of its antibacterial nature. Owing to the low removal efficiency of SMX in wastewater by activated sludge treatment process,[4] a large amount of SMX enters the environment annually. SMX has been detected in the effluents of sewage treatment plants as well as surface water, groundwater, and even tap water.[5] The concentration of SMX was detected as high as 2000 ng L^{-1} in many municipal sewage treatment plants and ranging from 30 to 480 ng L^{-1} in surface water.[6,7] Governments of different countries and researchers are getting aware of the discharged antibiotics and their by-products in nature water. Therefore, effective treatment techniques for enhancement of the SMX removal efficiency are urgently in need.

Advanced Oxidation Processes (AOPs) provide prospective procedures in degrading the refractory pollutants including POPs (persistent organic pollutants) and antibiotics.[8–17] In terms of the treatment of SMX, photolysis, photocatalysis, Fenton, ozonation, sulfate radicals-based processes, and ultrasonic process have been widely explored.[18–22] Among the treatment processes, sulfate radicals-based processes raised great interests in recent years because of its high efficiency, and less pH sensitivity.[23]

Peroxymonosulfate (PMS) was widely used as the oxidant to generate powerful sulfate radicals ($SO_4^{\bullet-}$).[23–26] It is comparatively

[a]Joint Laboratory of Guangdong Province and Hong Kong Region on Marine Bioresource Conservation and Exploitation, College of Marine Sciences, South China Agricultural University, Guangzhou, China. E-mail: marineymt@scau.edu.cn

[b]Department of Civil and Environmental Engineering, Hong Kong Polytechnic University, Hung Hom, Kowloon, Hong Kong. E-mail: wei.chu@polyu.edu.hk

[c]School of Chemical Engineering, ShengLi College, China University of Petroleum, Dongying, Shandong, China

† Electronic supplementary information (ESI) available. See DOI: 10.1039/d0ra05704e

 This journal is © The Royal Society of Chemistry 2020

Open Access Article. Published on 28 September 2020. Downloaded on 11/29/2025 9:39:57 AM.
This article is licensed under a Creative Commons Attribution-NonCommercial 3.0 Unported Licence.

more stable and easier to handle because of its solid state at ambient temperature.[27] Though using PMS directly to react with organics gives a slow reaction rate, PMS can be activated into highly reactive radicals by heat or transition metals *e.g.* Fe(II), the environmental friendly metal.[28] The limitation of coupling Fe(II) and PMS is its slow regeneration rate of Fe(II) from Fe(III), and UV irradiation may solve this drawback.[29]

Previous studies prove the high efficiency in SMX removal by processes based on sulfate radicals including UV + Persulfate, Thermo + Persulfate, Fe(II) + Persulfate, Benzoquinone + PMS, and Hydroxylamine + Fe(II) + PMS.[20,30–33] Despite the high efficiency, the treated SMX was reported to be more toxic for heat activated persulfate process.[34] Therefore, in case the degradation by-products of SMX possess toxicity to the aquatic environment, it is also essential to monitor the toxicity of the treated solution.

In this study, the process based on photo-assisted Fe(II) + PMS process was studied for SMX degradation. The effects of the parameters were investigated by evaluating the SMX removal under different light source, Fe(II) concentration, PMS concentration, and pH level. Prediction of degradation rate by varying SMX concentration was conducted. Besides, the reaction mechanism including mineralization, degradation products and pathways were determined and the toxicity of the treated solution was assessed.

2. Methodology

2.1 Chemicals and reagents

All chemicals are of analytic reagent grade and all solvents as mobile phases are of HPLC or LC/MS grade. SMX ($C_{10}H_{11}N_3O_3S$: 99.0%), PMS ($KHSO_5 \cdot 0.5KHSO_4 \cdot 0.5K_2SO_4$: 95%), and ferrous sulfate ($FeSO_4 \cdot 7H_2O$: 99.0%) were purchased from Sigma-Aldrich Inc. (USA). Sulfuric acid (H_2SO_4) and sodium hydroxide (NaOH) were used to adjust the initial pH of the solutions; monopotassium phosphate (KH_2PO_4), phosphate acid (H_3PO_4), and sodium nitrite ($NaNO_2$) were obtained from British Drug Houses (BDH, England). Acetonitrile (ACN, C_2H_3N), tertbutyl alcohol (TBA, $C_4H_{10}O$) and methanol (MeOH, CH_4O) were purchased from Tedia Company, USA. 1,10-Phenanthroline ($C_{12}H_{10}N_2O$) was obtained from International Laboratory (IL, USA). Ultrapure water generated from a Barnstead NANO pure water treatment system (Thermo Fisher Scientific Inc., USA) was employed for preparation of the solutions.

2.2 Experimental procedures

For SMX degradation, all experiments were performed in cylindrical borosilicate glass quartz beakers at 23 ± 2 °C. The beakers were placed on a magnetic stirrer at the center of a CCP-4V computer controlled photochemical reactor (Luzchem Research Inc.). Two phosphor-coated low-pressure mercury lamps emitting monochromatic light were symmetrically arranged on the top center within the reactor as the irradiation source. Four different types of lamps at 254, 300, 350 and 420 nm as UVC, UVB, UVA and VIS were investigated for the effect of light source. The power of the UV lamps was approximately 25 watts. The absorbance spectrum of relative energy of the UV lamps provided by the producer was shown in Fig. S1.†

The lamps were turned on 10 minutes before the start of the experiment for warming up and to ensure stable light irradiation. A cooling fan was installed in the reactor for temperature control. The fan was internally installed by the producer of the reactor. Therefore, the stable temperature (23 ± 2 °C) in the reactor can be ensured during the reaction and circulating cooling water was not needed. The reaction was initiated by the addition of predetermined amount of PMS and Fe(II) solution. The initial volume of each reaction solution was fixed at 400 mL. The beakers were stirred for a complete mixture and homogeneity throughout the reactions. Samples were taken at the preset time intervals and quenched with methanol (v/v = 1 : 1) for determination of the remaining SMX and transformation products. For TOC measurement, concentrated $NaNO_2$ was used as the quencher. For determination of the remaining Fe(II), samples of 1.5 mL were taken and mixed with 1.5 mL 1,10-phenanthroline. To identify the possible species in the reaction system, quenchers including TBA and MeOH were employed. The mole ratio of the quencher to PMS is 1000 : 1.

2.3 Analytical methods

The residual SMX was quantified by High Performance Liquid Chromatography (HPLC) which consists of a Waters 515 HPLC pump and a Waters 2487 UV detector. An isocratic flow running at a flow rate 1 mL min^{-1} was used with the mobile phase of ACN/10 mM monopotassium phosphate (50/50, pH adjustment to 3.0 with H_3PO_4). The injection volume was 10 μL. The UV detector wavelength was set at single wavelength at 258 nm. The retention time of SMX in this mobile phase was around 4.70 min. The peak area of detected SMX was recorded. Linear correlation was detected between varied SMX concentrations and the corresponding peak areas. SMX removal was presented in C/C_0, representing the normalized concentration with reference to the initial SMX concentration.

The identification of the transformation products was performed by the Ultra-High Performance Liquid Chromatography/Electrospray Ionization-Mass Spectrometry (UPLC/ESI-MS) system. The UPLC (Dionex UltiMate 3000) comprises a degasser, a pump, an autosampler, a diode array detector (DAD), a column compartment and a column (Thermo Hypersil GOLD, 1.9 μm, 50 × 2.1 mm). A gradient flow of the mobile phase containing ACN (A) and 0.1% formic acid (B) at 0.15 mL min^{-1} was employed. The injection volume was 5 μL. The ratio of A was kept at 10% during the first 2 min, then increased to 60% linearly during 2–15 min and held at 60% for 3 min. Finally, the ratio of mobile phase was returned to the initial composition until the end of the run. For mass analysis, alternative ion mode was employed. A Bruker amaZon SL ion trap mass analyzer coupled with an ion trap mass spectrometer detector (MSD) was performed.

TOC of the solution was measured with a TOC analyzer (Shimadzu, TOC-L). The concentration of Fe(II) was determined with a UV-vis spectrophotometer (MRC, Spectro UV-11) at 510 nm.

Open Access Article. Published on 28 September 2020. Downloaded on 11/29/2025 9:39:57 AM.
This article is licensed under a Creative Commons Attribution-NonCommercial 3.0 Unported Licence.

2.4 Toxicity test

The rotifer (*Brachionus calyciflorus*), an important aquatic species widely used in the toxicity assessment of pollutants, was employed for acute toxicity in this study. Toxicity testing was conducted using a 24-well polystyrene plate with the test solution adjusted to pH 7.0 ± 0.5. Ultrapure water was used as the culture medium for the control group and starve group. Ten healthy juveniles with age 0–2 h were selected into each well and exposed to the test sample of 1 mL for 24 h at 20 ± 0.5 °C in the dark. The green algae *Chlorella pyrenoidesa* of 50 μL was introduced as the food of rotifers to all groups except for the starve group. The survival of the rotifers was measured as the test parameter. Three replicates were performed for each group.

3. Results and discussion

3.1 Degradation of SMX in different systems

Fig. 1a presents the decay curves of SMX in different reaction systems. Only about 3% of SMX was degraded by UVA + PMS

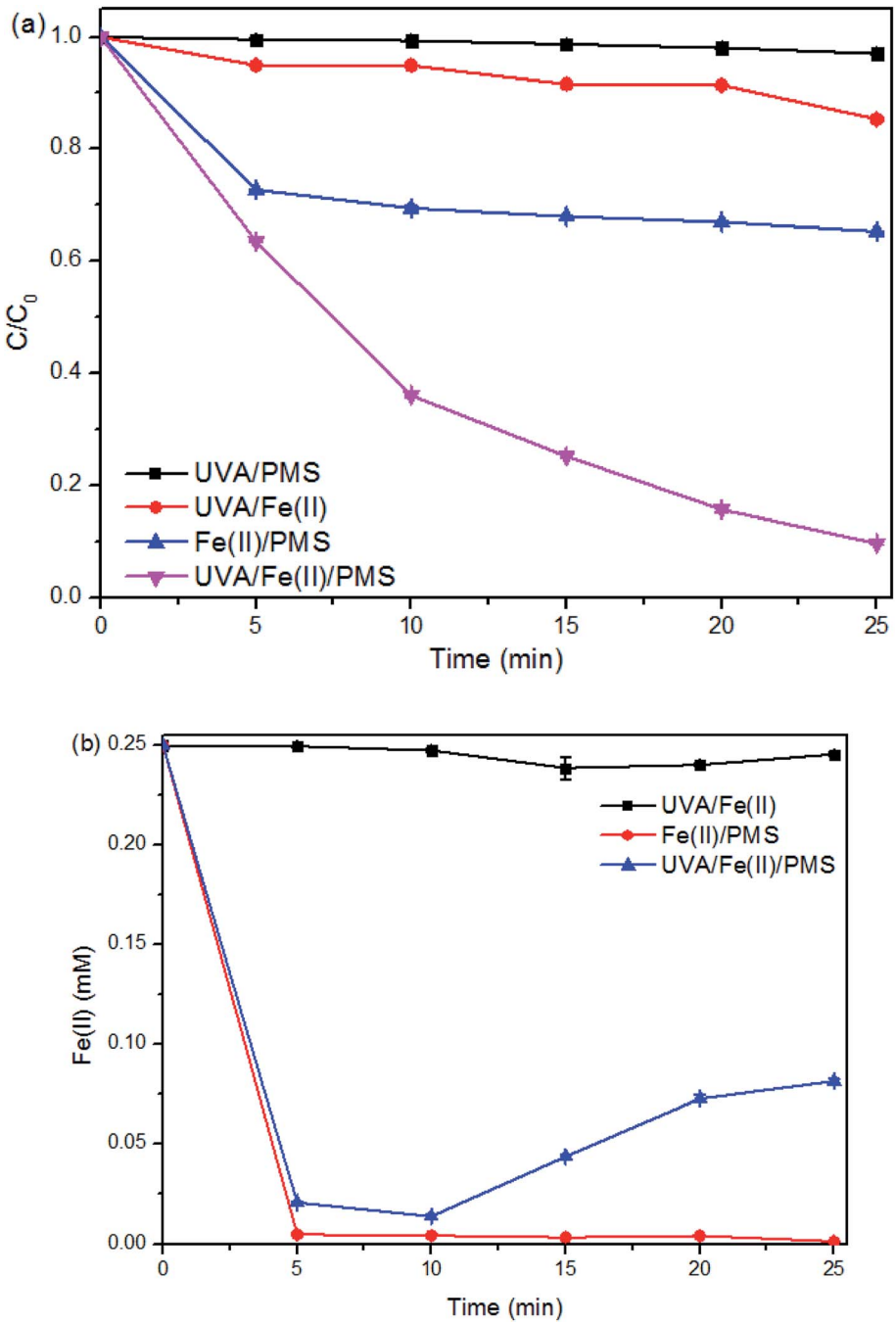

Fig. 1 SMX degradation in different reaction systems. (a) SMX decay curves. (b) Concentration change of Fe(II). Experimental conditions: $[SMX]_0 = 0.05$ mM, $[Fe(II)]_0 = 0.25$ mM, $[PMS]_0 = 0.25$ mM, $[pH]_0 = 6.09$, two UVA lamps were employed.

Open Access Article. Published on 28 September 2020. Downloaded on 11/29/2025 9:39:57 AM.
This article is licensed under a Creative Commons Attribution-NonCommercial 3.0 Unported Licence.

system, indicating that PMS could be slightly activated by UVA (eqn (1)).[35]

$$HSO_5^- \xrightarrow{h\nu} SO_4^{\cdot -} + OH\cdot \quad (1)$$

In the system of UVA + Fe(II), around 15% of SMX was removed within 25 min. As SMX degradation was negligible in the presence of sole UVA or sole Fe(II) (data not shown), the SMX degradation in this system was mainly due to the generation of $OH^{\cdot}$ from $[Fe(OH)]^{2+}$, a common species resulting from the hydrolysis of Fe(III) (eqn (2)–(4)).[36] From Fig. 1b, the concentration of Fe(II) kept unchanged throughout the whole reaction because of the Fe(II)/Fe(III) cycle in the presence of UVA.

$$Fe^{2+} \xrightarrow{h\nu} Fe^{3+} + e^- \quad (2)$$

$$Fe^{3+} + H_2O \rightarrow [Fe(OH)]^{2+} + H^+ \quad (3)$$

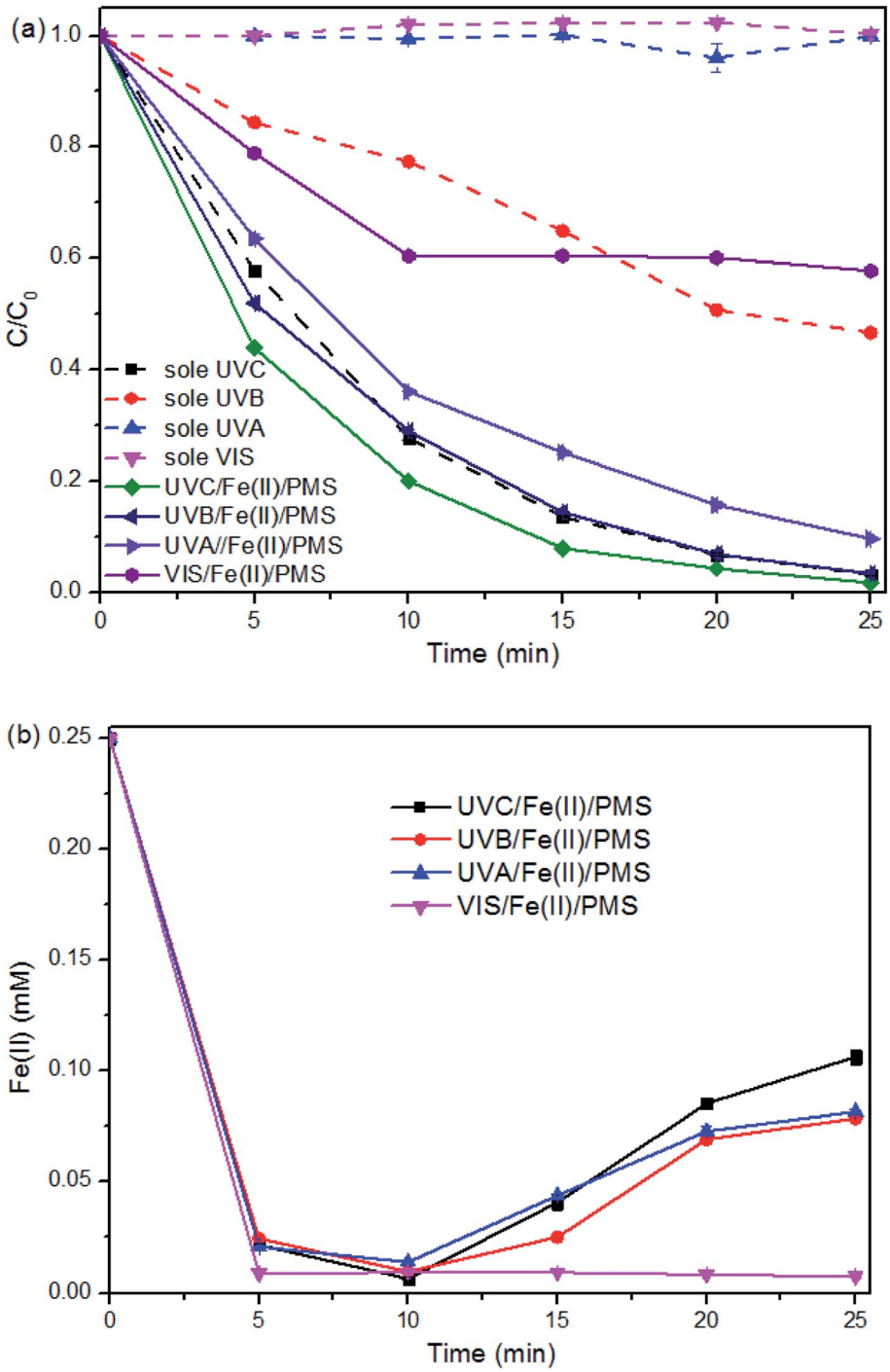

Fig. 2 SMX degradation in the Fe(II) + PMS system with varied light source. (a) SMX decay curves. (b) Concentration change of Fe(II). Experimental conditions: $[SMX]_0 = 0.05$ mM, $[PMS]_0 = 0.25$ mM, $[Fe(II)]_0 = 0.25$ mM, $[pH]_0 = 6.09$, two lamps were employed.

Open Access Article. Published on 28 September 2020. Downloaded on 11/29/2025 9:39:57 AM.
This article is licensed under a Creative Commons Attribution-NonCommercial 3.0 Unported Licence.

$$[Fe(OH)]^{2+} \xrightarrow{h\nu} Fe^{2+} + OH^{\cdot} \quad (4)$$

Compared to UVA, Fe(II) is more effective in activating PMS, with a SMX removal of 35% achieved within 25 min in the system of PMS + Fe(II). Besides, the possible involvement of $Fe(IV)O_2^+$ in the reaction system PMS + Fe(II) may also contribute to the relatively higher removal efficiency.[37] The SMX degradation is much more significant in the first 5 minutes (with approximately 30% removal efficiency) than that in the following 20 minutes (with only about 5% additional removal). From Fig. 1b, the concentration of Fe(II) was decreased during the process because of the activation of PMS (to form sulfate radicals) and the transformation to Fe(III), simultaneously. Fe(II) was used up during the first 5 minutes, and cannot be regenerated from the beneficial Fe(II)/Fe(III) cycle without the

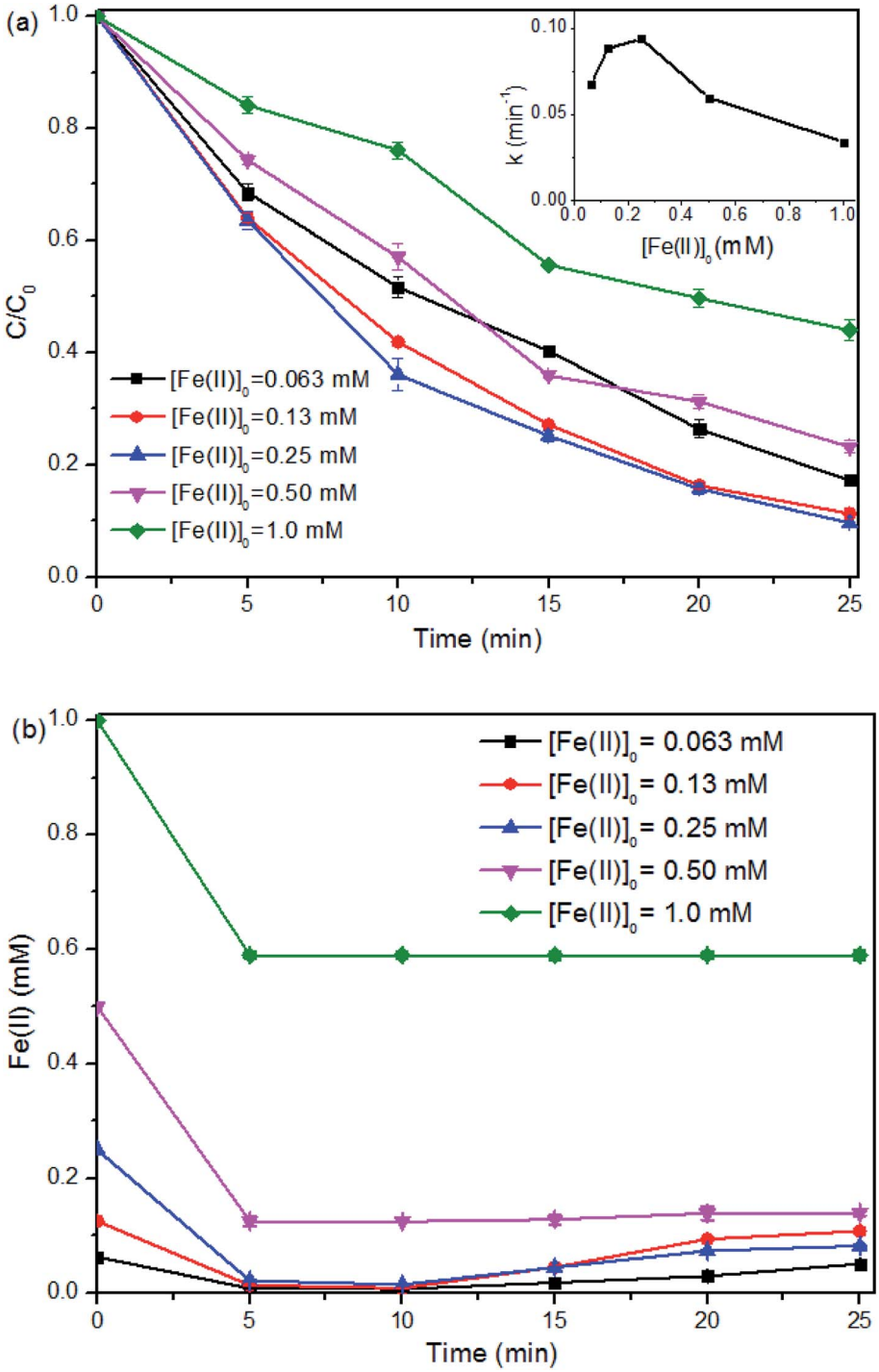

Fig. 3 Effect of Fe(II) concentration on SMX degradation in the Fe(II) + PMS + UVA system. (a) SMX degradation. (b) Concentration change of Fe(II). Experimental conditions: $[SMX]_0 = 0.05$ mM, $[PMS]_0 = 0.25$ mM, $[pH]_0 = 6.09$, two UVA lamps were employed.

Open Access Article. Published on 28 September 2020. Downloaded on 11/29/2025 9:39:57 AM.
This article is licensed under a Creative Commons Attribution-NonCommercial 3.0 Unported Licence.

assistant of UVA. Because of the approaching of complete consumption of both Fe(II) and PMS, the reaction was retarded afterwards.

$$Fe^{2+} + HSO_5^- \rightarrow SO_4^{\bullet -} + Fe^{3+} + OH^- \quad (5)$$

The removal efficiency of SMX in the UVA + Fe(II) + PMS system is substantially higher than those in the above systems. It is shown in Fig. 1a that the degradation process possesses a relatively stable curve during the 25 minute reaction time, which corresponds to the pseudo first-order kinetics. In this system, $SO_4^{\bullet -}$ can be formed through the activation of PMS by either Fe(II) or UVA (eqn (1) and (2)). And $OH^{\bullet}$ can be formed through the activation of PMS or Fe(II) by UVA (eqn (1), (3)–(5)). Though Fe(II) can be transformed to Fe(III) by both UVA and PMS, the remaining of [Fe(II)] at the 5th min (0.025 mM) is apparently high enough to maintain a healthy continuity of the process compared to that of the depletion of Fe(II) in the dark system. The regeneration of Fe(II) from Fe(III) due to the presence of UVA is apparently the key (Fig. 1b).

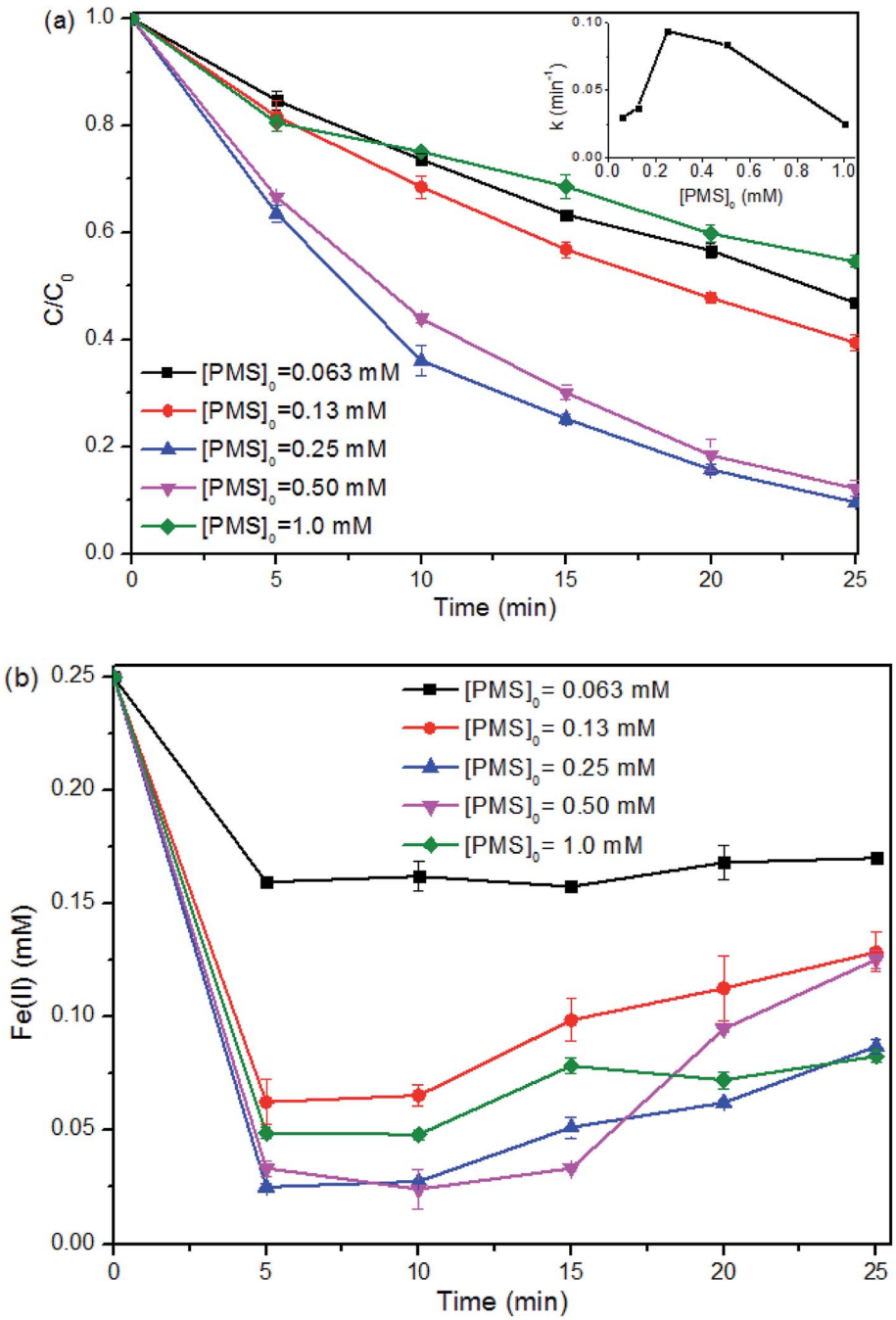

Fig. 4 Effect of PMS concentration on SMX degradation in the Fe(II) + PMS + UVA system. (a) SMX degradation. (b) Concentration change of Fe(II). Experimental conditions: $[SMX]_0 = 0.05$ mM, $[Fe(II)]_0 = 0.25$ mM, $[pH]_0 = 6.09$, two UVA lamps were employed.

Open Access Article. Published on 28 September 2020. Downloaded on 11/29/2025 9:39:57 AM.
This article is licensed under a Creative Commons Attribution-NonCommercial 3.0 Unported Licence.

3.2 SMX degradation in Fe(II) + PMS system activated with different light sources

The contribution of hydrolysis to the SMX degradation was evaluated and proven to be insignificant in this study (data not shown). However, SMX removal efficiency *via* direct photolysis under UVC and UVB was found to be 97% and 55%, respectively (Fig. 2a). Direct photolysis was not helpful for TOC removal[21] and the shortwave UV is not available in the sunlight, thus UVC and UVB was not recommended for SMX degradation.

The direct photolysis of SMX under UVA and VIS was insignificant due to their low energy and the lower absorption of SMX at higher range of the light wavelength. However, the degradation performance under UVA + Fe(II) + PMS process is much better than that under VIS + Fe(II) + PMS. For the treatment process VIS + Fe(II) + PMS, SMX degradation was limited to the initial 10 min and being retarded afterward, indicating the limited ability of VIS to activate Fe(II) + PMS.

The limited ability was also illustrated from Fig. 2b, where the [Fe(II)] evolution in the VIS + Fe(II) + PMS was similar to that in the Dark + Fe(II) + PMS. While the [Fe(II)] evolution in the UV + Fe(II) + PMS systems, despite the wavelength, shows similar patterns. Therefore, the regeneration of Fe(II) can be realized under the irradiation of UV. As UVA also has the potential for using solar light as the free energy source, UVA + Fe(II) + PMS was further investigated for the SMX degradation in this study.

3.3 SMX degradation performance in the Fe(II) + PMS + UVA system

3.3.1 Effect of the reagents on SMX degradation. The reaction rates of SMX degradation with varied concentrations of reagents were calculated according to the pseudo first-order kinetics (Fig. 3a). As the concentration of Fe(II) ([Fe(II)]) increased from 0.0625 to 0.25 mM, the reaction rate increased from 0.0675 to 0.0937 min^{-1}, but then gradually decreased to 0.0341 min^{-1} as the [Fe(II)] continued to increase to 1.00 mM. Therefore, the optimal dosage of the reagent Fe(II) in this study is determined to be 0.25 mM. It's interesting to note that for the reactions with $[Fe(II)]_0$ at or lower than 0.25 mM, Fe(II) was exhausted quickly (Fig. 3b). This means Fe(II) as the limiting factor, the insufficient of Fe(II) would lead to deficient radicals generated. Under these circumstance, the untouched PMS in the solution may actively play the role as scavenger, which terminates the precious sulfate radicals into SO_4^{2-} (eqn (6)).[38] After the rapid drop of [Fe(II)] in the first 5 min, a steady stage of [Fe(II)] was followed in the next 5 min, which may be attributed to the balance of consumption and regeneration of Fe(II). Afterwards, [Fe(II)] increased likely due to the excess of Fe(II) regeneration than its consumption.

As $[Fe(II)]_0$ was overdosed at or above 0.50 mM, it is interesting to note that, around 0.40 mM of Fe(II) ($[Fe(II)]_\Delta$) was consumed with a fixed $[PMS]_0$ at 0.25 mM in 5 min of the reaction regardless of the $[Fe(II)]_0$ (*i.e.*, $[Fe(II)]_\Delta : [PMS]_0$ = 1.6 : 1). In this case, a large amount of free Fe(II) was left in the solution and resulted in additional scavenging effect (eqn (7) and (8)).[29,39] The sulfate radicals and hydroxyl radicals may be transformed by the overdosed Fe(II) to SO_4^{2-} and OH^-, respectively.[27]

$$HSO_5^- + SO_4^{\bullet-} \rightarrow SO_5^{\bullet-} + SO_4^{2-} + H^+ \quad (6)$$

$$Fe^{2+} + SO_4^{\bullet-} \rightarrow Fe^{3+} + SO_4^{2-} \quad (7)$$

$$Fe^{2+} + OH^{\bullet} \rightarrow Fe^{3+} + OH^- \quad (8)$$

Similarly, the SMX removal was enhanced within the $[PMS]_0$ from 0.0625 to 0.25 mM and then reduced with the continue increase of $[PMS]_0$ (Fig. 4a). As can be seen from Fig. 4b, for the reactions with $[PMS]_0$ lower than 0.25 mM, the reaction ratio of $[Fe(II)]_\Delta : [PMS]_0$ at the first 5 min was also 1.6 : 1. However, higher $[PMS]_0$ at 0.25 mM or above was unable to react with [Fe(II)] effectively, with around 0.20 mM Fe(II) consumed. Low dosage of PMS means insufficient radicals, as well as surplus Fe(II) leading to scavenging effect (eqn (6) and (7)). While overdosed PMS increases the chance to quench the radicals (eqn (5)). Therefore, the properly adjusted $[Fe(II)]_0$ and $[PMS]_0$ played a critical role in SMX degradation. Relatively lower or higher Fe(II)/PMS would retard the reaction, and the optimal ratio of $[Fe(II)]_0 : [PMS]_0$ for SMX degradation in this study was determined at 1 : 1.

3.3.2 Effect of pH. The pH level shows significant effect on SMX degradation performance. As shown in Fig. 5, the optimum pH for SMX degradation was determined to be around 6.0, where the fastest decay rate and highest overall removal were observed.

The removal efficiency of SMX was enhanced significantly with the increase of the initial pH from 2.07 to 6.09. Previous studies stated that the free Fe(II) was reduced in extremely acidic condition or at high pH levels due to the formation of $[Fe \cdot H_2O]^{2+}$ or $Fe(OH)_2$, respectively.[40] Besides, large amount of H^+ could plays the role of $SO_4^{\bullet-}$ scavenger,[41] extremely low pH was not favorable for SMX removal in this process. With further increase of pH to 9.27, SMX decay was significantly retarded, with final removals around 40%. In alkaline conditions, the self-

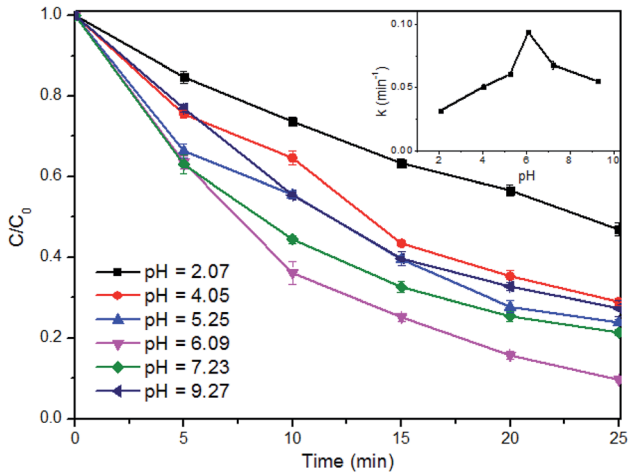

Fig. 5 Effect of pH on SMX degradation in the Fe(II) + PMS + UVA system. Experimental conditions: $[SMX]_0$ = 0.05 mM, $[Fe(II)]_0$ = 0.25 mM, $[PMS]_0$ = 0.25 mM, two UVA lamps were employed.

Open Access Article. Published on 28 September 2020. Downloaded on 11/29/2025 9:39:57 AM.
This article is licensed under a Creative Commons Attribution-NonCommercial 3.0 Unported Licence.

dissociation may occur to PMS, and the active oxygen of PMS starts to decompose.[42,43] This would lead to less sulfate radicals available for SMX degradation, and thus inhibited SMX degradation at high pH levels. Therefore, the pH level of around 6.0 is recommended for SMX degradation, which is also a great advantage of the proposed process for real application.

3.3.3 Prediction of degradation rate with varied initial concentration of SMX. To investigate the application of pseudo first-order kinetic equation and the degradation capability of SMX, wide range of initial SMX concentration ($[SMX]_0$) was selected. As is shown in Fig. 6, SMX degradation with all the investigated concentrations followed pseudo first-order reactions. The removal efficiency or decay rate of SMX was reduced with the increase of $[SMX]_0$ as the $[Fe(II)]_0$ and $[PMS]_0$ were fixed at 0.25 mM. It is reasonable that higher dosages of radicals were required to remove more SMX molecules. When the dosages of

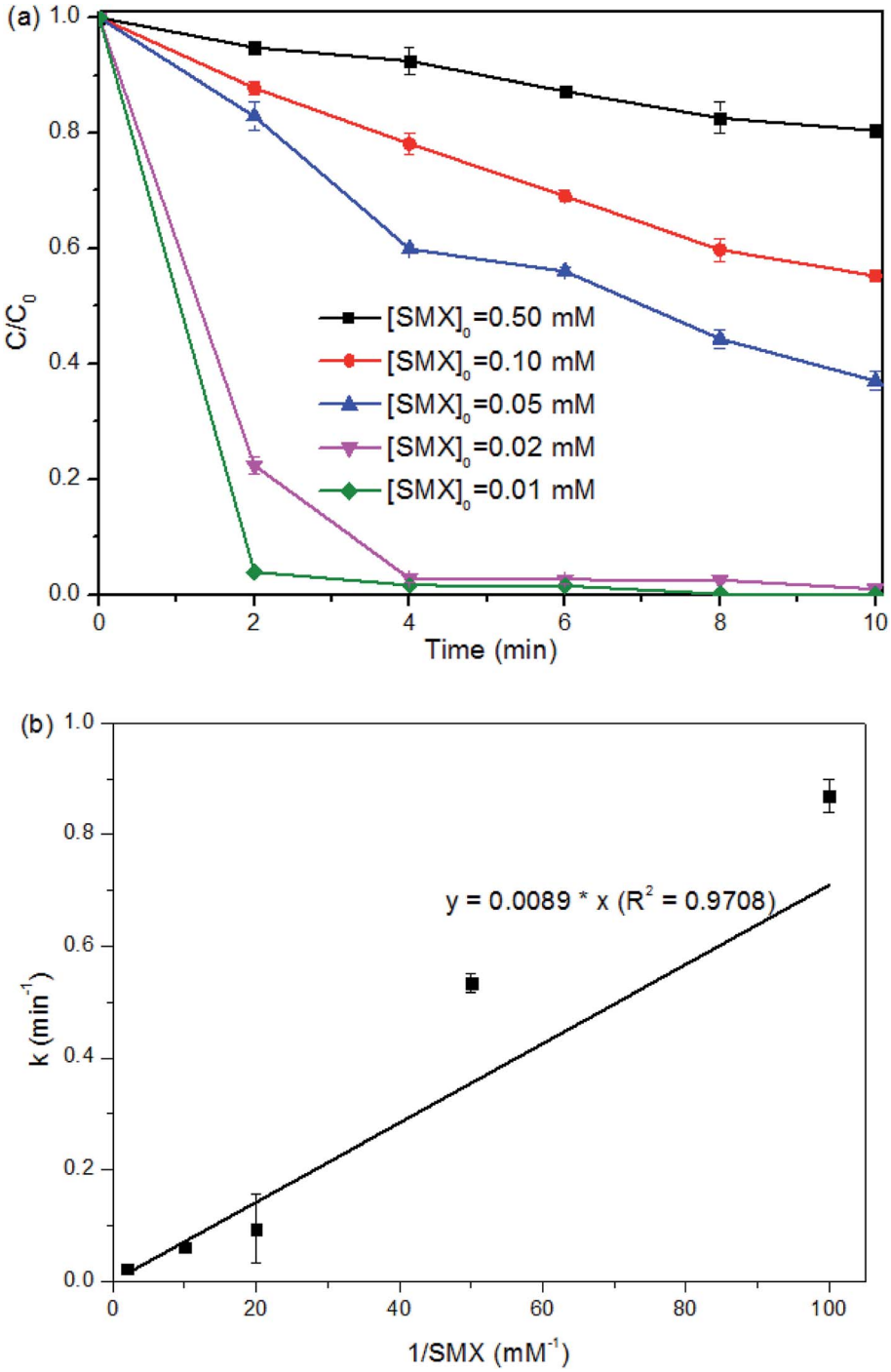

Fig. 6 Prediction of kinetics with varied SMX concentration in the Fe(II) + PMS + UVA system. Experimental conditions: $[Fe(II)]_0 = 0.25$ mM, $[PMS]_0 = 0.25$ mM, $[pH]_0 = 6.09$, two UVA lamps were employed.

Open Access Article. Published on 28 September 2020. Downloaded on 11/29/2025 9:39:57 AM.
This article is licensed under a Creative Commons Attribution-NonCommercial 3.0 Unported Licence.

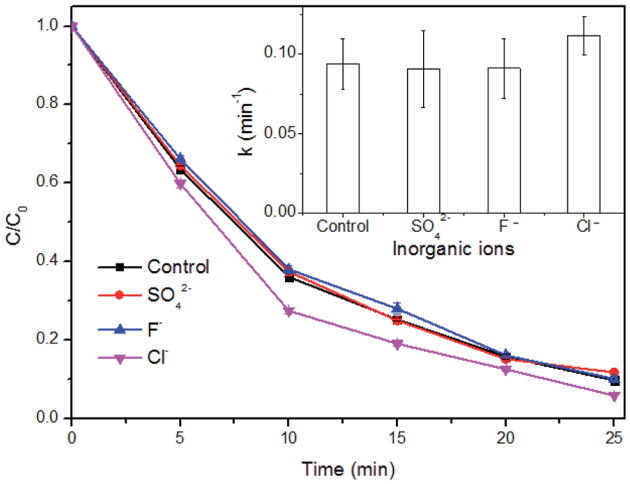

Fig. 7 Effect of inorganic ions on SMX degradation by Fe(II) + PMS + UVA process. Experimental conditions: $[Fe(II)]_0$ = 0.25 mM, $[PMS]_0$ = 0.25 mM, $[Ion]_0$ = 0.10 mM, $[pH]_0$ = 6.09, two UVA lamps were employed.

the reagents and the UVA intensity were fixed, the radicals generated would be deficient at higher $[SMX]_0$. From Fig. 6, the degradation rate at varied $[SMX]_0$ was determined. A linear correlation between the reaction rate constant k and $[SMX]_0^{-1}$ was established, hence the k values can be predicated with varied $[SMX]_0$.

$$k = 0.0089/[SMX]_0 \ (R^2 = 0.9708) \tag{9}$$

3.3.4 Effect of anions. The effect of the inorganic anions including Cl^-, F^- and SO_4^{2-} on the performance of the process was studied. From Fig. 7, it was observed that F^- and SO_4^{2-} had no significant influence on SMX degradation. Though Cl^- has similar chemical property with F^-, it showed different effect on SMX degradation. SMX degradation was accelerated with the presence of Cl^-. The positive effect was possibly due to the generation of chlorine and hypochlorous acid (eqn (10) and (11))[44] which had good potential of removing SMX[45] and the intermediates. Besides, a pervious study showed that Cl^- could activate PMS to remove the azo dye Acid Orange 7.

$$2Cl^- \rightarrow Cl_2 + 2e^- \tag{10}$$

$$Cl_2 + H_2O \rightarrow HOCl + Cl^- + H^+ \tag{11}$$

3.4 Reaction mechanism of SMX degradation

3.4.1 Proposed intermediates and pathways. During SMX degradation under the treatment process UVA + Fe(II) + PMS, six intermediates including $\mathbf{C_{269}}$, $\mathbf{C_{283}}$, $\mathbf{C_{162}}$, $\mathbf{C_{98}}$, $\mathbf{C_{294}}$, and $\mathbf{C_{345}}$ were detected by UPLC/ESI-MS (Fig. 8a). The structures of the intermediates were determined based on the MS/MS2 spectrum (Fig. S2†). The detailed information including detention time and detection mode of the intermediates was displayed in Table S1.† Compared to previous studies, $\mathbf{C_{269}}$ and $\mathbf{C_{98}}$ were frequently detected in other treatment processes. While four of the proposed intermediates including $\mathbf{C_{283}}$, $\mathbf{C_{162}}$, $\mathbf{C_{294}}$, and $\mathbf{C_{345}}$ were newly reported.

The product $\mathbf{C_{269}}$ (m/z = 269.82 for $[M + H]^+$), increasing by 16 mass units from the parent compound SMX, suggests the addition of one hydroxyl group to SMX. The location of the hydroxyl group cannot be confirmed due to the insufficient information provided in the MS/MS2 spectrum. The presence of $\mathbf{C_{269}}$ was also detected during SMX degradation by ultrasound + ozone oxidation,[22] thermo + persulfate oxidation,[32] ferrate oxidation,[46] ferrate + US process,[47] and Fe(II) + montmorillonite catalyzed ozonation.[48]

$\mathbf{C_{283}}$, at m/z 283.83 in positive ion mode, was supposed to result from the carboxylation of the methyl group on the isoxazole ring. The variation of 30 mass units from the parent compound SMX, was proposed to come from the introduction of two oxygen molecular, as well as the loss of two hydrogen molecular. The amino group on the benzene ring of $\mathbf{C_{283}}$ was confirmed by the mass difference of 91 units between the product ion at m/z 283.82 and that at m/z 192.70.

The intermediate $\mathbf{C_{162}}$ detected in negative ion mode was proposed to result from the loss of the benzene ring (together with the amino group) from the parent compound.

The intermediate $\mathbf{C_{98}}$ was proposed to result from the bond cleavage of S–N between sulfonyl and benzene ring. It was also detected in SMX degradation by treatment processes including Fe(II) + persulfate[49] and UV + H_2O_2.[18]

The species $\mathbf{C_{294}}$, with m/z 293.08 in negative ion mode, differing by 40 mass units from the SMX molecular, was attributed to the addition of two hydroxyl groups, as well as the oxidation of the benzene ring. The product ion at m/z 201.68, corresponding to loss of 92 units from the product ion at m/z 293.08, was obtained from the loss of the isoxazole and one amino group. The product ions at m/z 235.87 in the MS2 spectra, with variation of around 57 mass units from m/z 293.08, was proposed to be $-CH_2COOH$ group formed from the oxidation of the benzene ring.

The MS data which shows the fragment ion at m/z 344.08 in negative ion mode suggests the introduction of groups with mass 92 based on the parent compound (m/z 253.83). The fragment at m/z 313.04, with difference value of 64 units m/z from the fragment ion at m/z 247.79 shown from MS2 data, indicates four hydroxyl groups. And the remaining mass difference of 28 indicates the addition of –CO group. Therefore, the intermediate $\mathbf{C_{345}}$ comes from the introduction of four hydroxyl groups, as well as the transformation of $-NH_2$ to $-NH_2CO$ on the benzene ring. The latter one may be obtained from the combination of the $-NH_2$ group with the –HCOOH group from the formic acid, a common product formed during AOPs.

According to the proposed intermediates, carboxylation, hydroxylation, isoxazole ring opening, loss of benzene ring, N–S cleavage and dehydration condensation were illustrated as SMX degradation pathways under the process UVA + Fe(II) + PMS (Fig. 8a).

Open Access Article. Published on 28 September 2020. Downloaded on 11/29/2025 9:39:57 AM.
This article is licensed under a Creative Commons Attribution-NonCommercial 3.0 Unported Licence.

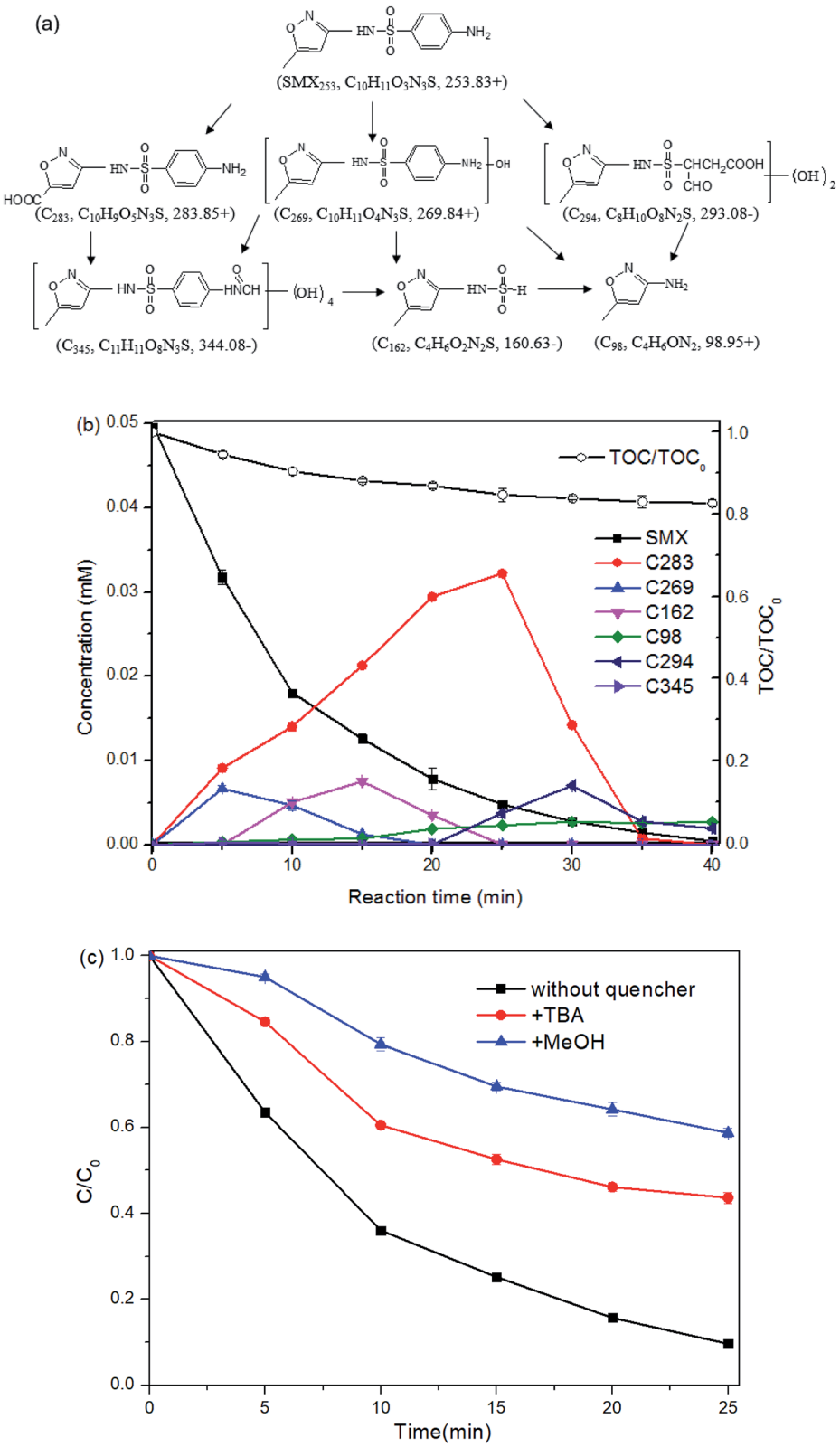

Fig. 8 Reaction mechanism of SMX degradation in the Fe(II) + PMS + UVA system. (a) Proposed degradation pathways. (b) TOC reduction and proposed concentration of the degradation products. (c) SMX degradation with quenchers. Experimental conditions: $[SMX]_0 = 0.05$ mM, $[Fe(II)]_0 = 0.25$ mM, $[PMS]_0 = 0.25$ mM, $[pH]_0 = 6.09$, two UVA lamps were employed.

Open Access Article. Published on 28 September 2020. Downloaded on 11/29/2025 9:39:57 AM.
This article is licensed under a Creative Commons Attribution-NonCommercial 3.0 Unported Licence.

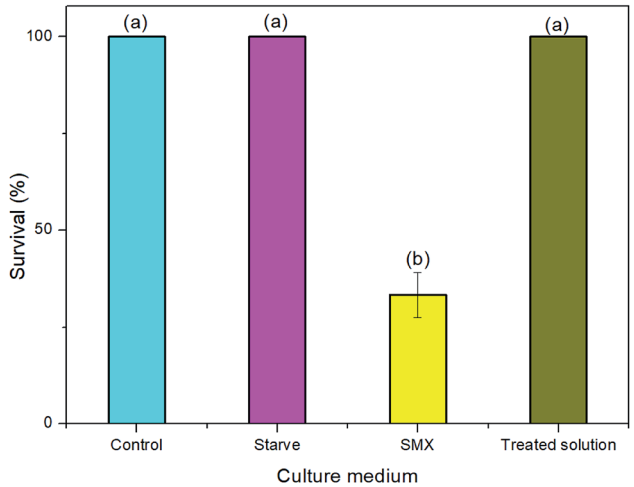

Fig. 9 The effect of SMX solution to rotifers before and after treatment. Treatment conditions: $[SMX]_0 = 0.05$ mM, $[Fe(II)]_0 = 0.25$ mM, $[PMS]_0 = 0.25$ mM, $[pH]_0 = 6.09$, two UVA lamps were employed.

3.4.2 Mineralization and proposed concentration of the generated intermediates. During SMX degradation, only about 17% TOC reduction was reached as SMX was removed completely (Fig. 8b). From the proposed degradation pathway, the TOC reduction was mainly due to isoxazole ring opening, loss of benzene ring, and N–S cleavage.

The peak areas of the detected intermediates from the chromatography were recorded in Fig. S3.† As the standards of these generated intermediates were not available from the market, it is impractical to provide the exact concentrations of each intermediates. According to the structures of the detected intermediates and the low TOC reduction, it was assumed that no isoxazole-ring was opened at the initial stage and hence the isoxazole-ring balance was followed during the reaction. Besides, the concentrations of the intermediates are assumed to be linear to the corresponding areas from the chromatographic peaks based on the Beer–Lambert law. Then the concentration of the detected intermediates may be proposed with the following equation.

$$A_{SMX(t=0)} = A_{SMX(t_x)} + \frac{A_{int_1(t_x)}}{\S_{int_1}/\S_{SMX}} + \frac{A_{int_2(t_x)}}{\S_{int_1}/\S_{SMX}} \ldots + \frac{A_{int_n(t_x)}}{\S_{int_n}/\S_{SMX}} \quad (12)$$

where A_{SMX} and A_{int} represents the peak area of the parent compound (*i.e.*, SMX) and the intermediate, respectively. The $\S_{SMX}$ and $\S_{int}$ is the molar absorptivity of SMX and the intermediate, respectively.

Six formulas were built up as the experiment data (A_{SMX} and A_{int} at 5, 10, 15, 20, 25, and 30 min) were put into the above eqn (12). The unknown values of $\S_{SMX}/\S_{int}$ for $\mathbf{C_{283}}$, $\mathbf{C_{269}}$, $\mathbf{C_{162}}$, $\mathbf{C_{98}}$, $\mathbf{C_{294}}$ and $\mathbf{C_{345}}$ are solved to be 0.67, 1.05, 1.52, 3.23, 1.32 and 3.47, respectively. Therefore, the concentration of the intermediate can be determined and the result was shown in Fig. 8b.

3.4.3 Identification of the reactive species. TBA scavenged $OH^{\bullet}$ radicals and MeOH scavenged both of $OH^{\bullet}$ and $SO_4^{\bullet-}$ radicals.[50] From Fig. 8c, around 33% decrease of SMX removal efficiency was observed as the radicals $OH^{\bullet}$ were quenched, and additional 25% decrease was detected by further quench of $SO_4^{\bullet-}$. The result suggests the involvement of both $OH^{\bullet}$ and $SO_4^{\bullet-}$ radicals during SMX degradation, and $OH^{\bullet}$ radicals contributed more to SMX degradation.

3.5 Toxicity of the treated solution to rotifers

The survival of the rotifers was threatened by SMX solution, only around 30% rotifers survived as exposed to 0.05 mM SMX. After treatment for 40 min, the parent compound was removed completely (at least the concentration was lower than the detection limitation of LC). Though only around 17% TOC reduction was reached, only two intermediates ($\mathbf{C_{98}}$ and $\mathbf{C_{294}}$ at around 0.002 mM) were detected at the 40th min of the treatment. Though higher toxicity of $\mathbf{C_{98}}$ was predicted by ECOSAR in previous studies by Yang *et al.*, and Milh *et al.*,[20,51] no adverse effect of $\mathbf{C_{98}}$ at 5.6 mM was detected by testing growth inhibition of *Vibrio fischeri* by Majewsky *et al.*[52] In this study, the solution after treatment for 40 min showed no significant difference compared to that in control group (Fig. 9). Though the toxicity of $\mathbf{C_{294}}$ was unknown, the result indicates the mixture of $\mathbf{C_{98}}$ and $\mathbf{C_{294}}$ at around 0.002 mM was safe to the survival of rotifers. Taking into consideration of the residual 87% TOC, it can be predicted that the undetected low-molecular organic substances have no significant adverse effect on the survival of rotifers. Therefore, it is believed that the treatment process was efficient to transform the toxic SMX to harmfulless substances.

4. Conclusion

In this study, SMX was removed efficiently under the treatment process UVA + Fe(II) + PMS. The performance of the treatment process was affected by operating parameters such as the concentration of [Fe(II)], [PMS], and the pH level of solution. The optimum SMX degradation efficiency was observed in the pH level of around 6.0, with [Fe(II)] : [PMS] = 1 : 1. A model was established to predict the removal efficiency or reaction rate in terms of the initial concentration of SMX. Six transformation products and the corresponding concentrations were proposed. Around 17% TOC reduction was reached as SMX was removed completely. Carboxylation, hydroxylation, isoxazole ring opening, loss of benzene ring, N–S cleavage and dehydration condensation were involved as the degradation pathways. The radicals $OH^{\bullet}$ and $SO_4^{\bullet-}$ were involved and $OH^{\bullet}$ contributed more to SMX degradation. The treated SMX showed no acute toxicity to the tested rotifers. This study provided an efficient method to remove SMX.

Conflicts of interest

There are no conflicts to declare.

Acknowledgements

This study was funded by the National Natural Science Foundation of China (41807476), Science and Technology Program of

Open Access Article. Published on 28 September 2020. Downloaded on 11/29/2025 9:39:57 AM.
This article is licensed under a Creative Commons Attribution-NonCommercial 3.0 Unported Licence.

Guangdong, China (2019A141405034) and Hong Kong Polytechnic University (1-ZVH6).

References

1 H. Xie, H. Hao, N. Xu, X. Liang, D. Gao, Y. Xu, Y. Gao, H. Tao and M. Wong, *Sci. Total Environ.*, 2019, **659**, 230–239.
2 M. Isidori, M. Lavorgna, A. Nardelli, L. Pascarella and A. Parrella, *Sci. Total Environ.*, 2005, **346**, 87–98.
3 G. G. Ying, L. Y. He, A. J. Ying, Q. Q. Zhang, Y. S. Liu and J. L. Zhao, *Environ. Sci. Technol.*, 2017, **51**, 1072–1073.
4 P. Verlicchi, M. Al Aukidy and E. Zambello, *Sci. Total Environ.*, 2012, **429**, 123–155.
5 A. Puckowski, K. Mioduszewska, P. Lukaszewicz, M. Borecka, M. Caban, J. Maszkowska and P. Stepnowski, *J. Pharm. Biomed. Anal.*, 2016, **127**, 232–255.
6 T. B. Minh, H. W. Leung, I. H. Loi, W. H. Chan, M. K. So, J. Q. Mao, D. Choi, J. C. Lam, G. Zheng, M. Martin, J. H. Lee, P. K. Lam and B. J. Richardson, *Mar. Pollut. Bull.*, 2009, **58**, 1052–1062.
7 A. L. Spongberg, J. D. Witter, J. Acuna, J. Vargas, M. Murillo, G. Umana, E. Gomez and G. Perez, *Water Res.*, 2011, **45**, 6709–6717.
8 M. J. Chen, Y. Huang and W. Chu, *Chin. J. Catal.*, 2019, **40**, 673–680.
9 L. Xu, Y. Sun, L. Gan, J. Han, P. Wang, L. Yu, X. Mei, W. Li, B. Lyu, C. Pei and W. Chu, *Appl. Catal., B*, 2019, **259**, 117958.
10 M. J. Chen and W. Chu, *Chem. Eng. J.*, 2016, **296**, 310–318.
11 A. Hassani, A. Khataee, S. Karaca and M. Fathinia, *RSC Adv.*, 2016, **6**, 87569–87583.
12 F. Ghanbari, M. Riahi, B. Kakavandi, X. Hong and K.-Y. A. Lin, *J. Water Process. Eng.*, 2020, **36**, 101321.
13 F. Ghanbari, F. Zirrahi, K.-Y. A. Lin, B. Kakavandi and A. Hassani, *J. Environ. Chem. Eng.*, 2020, **8**, 104167.
14 F. Ghanbari, F. Zirrahi, D. Olfati, F. Gohari and A. Hassani, *J. Mol. Liq.*, 2020, **310**, 113217.
15 A. Hassani, M. Faraji and P. Eghbali, *J. Photochem. Photobiol., A*, 2020, **400**, 112665.
16 A. Hassani, A. Khataee, M. Fathinia and S. Karaca, *Process Saf. Environ. Prot.*, 2018, **116**, 365–376.
17 P. Y. Motlagh, A. Khataee, A. Hassani and T. Sadeghi Rad, *J. Mol. Liq.*, 2020, **302**, 112532.
18 R. Zhang, Y. Yang, C. H. Huang, N. Li, H. Liu, L. Zhao and P. Sun, *Environ. Sci. Technol.*, 2016, **50**, 2573–2583.
19 H. W. Yu, T. Anumol, M. Park, I. Pepper, J. Scheideler and S. A. Snyder, *Water Res.*, 2015, **81**, 250–260.
20 Y. Yang, X. Lu, J. Jiang, J. Ma, G. Liu, Y. Cao, W. Liu, J. Li, S. Pang, X. Kong and C. Luo, *Water Res.*, 2017, **118**, 196–207.
21 H. Y. Kim, T. H. Kim and S. Yu, *J. Environ. Sci. Health, Part A: Toxic/Hazard. Subst. Environ. Eng.*, 2015, **50**, 292–300.
22 W. Q. Guo, R. L. Yin, X. J. Zhou, J. S. Du, H. O. Cao, S. S. Yang and N. Q. Ren, *Ultrason. Sonochem.*, 2015, **22**, 182–187.
23 L. J. Xu, W. Chu and L. Gan, *Chem. Eng. J.*, 2015, **263**, 435–443.
24 L. Gan, Q. Zhong, A. Geng, L. Wang, C. Song, S. Han, J. Cui and L. Xu, *Sci. Total Environ.*, 2019, **694**, 133705.
25 L. Xu, X. Wang, Y. Sun, H. Gong, M. Guo, X. Zhang, L. Meng and L. Gan, *Ultrason. Sonochem.*, 2019, **60**, 104749.
26 Y. Rao, F. Han, Q. Chen, D. Wang, D. Xue, H. Wang and S. Pu, *Chemosphere*, 2019, **218**, 299–307.
27 Y. R. Wang and W. Chu, *Chem. Eng. J.*, 2013, **215–216**, 643–650.
28 L. Xu, L. Meng, X. Zhang, X. Mei, X. Guo, W. Li, P. Wang and L. Gan, *J. Hazard. Mater.*, 2019, **379**, 120795.
29 Y. R. Wang and W. Chu, *Appl. Catal., B*, 2012, **123–124**, 151–161.
30 Y. Zhou, J. Jiang, Y. Gao, J. Ma, S. Y. Pang, J. Li, X. T. Lu and L. P. Yuan, *Environ. Sci. Technol.*, 2015, **49**, 12941–12950.
31 G. Liu, X. Li, B. Han, L. Chen, L. Zhu and L. C. Campos, *J. Hazard. Mater.*, 2017, **322**, 461–468.
32 Y. Ji, Y. Fan, K. Liu, D. Kong and J. Lu, *Water Res.*, 2015, **87**, 1–9.
33 Y. Ji, C. Ferronato, A. Salvador, X. Yang and J. M. Chovelon, *Sci. Total Environ.*, 2014, **472**, 800–808.
34 Y. Q. Gao, N. Y. Gao, Y. Deng, D. Q. Yin, Y. S. Zhang, W. L. Rong and S. D. Zhou, *Desalin. Water Treat.*, 2014, **56**, 2225–2233.
35 E. Hayon, A. Treinin and J. Wilf, *J. Am. Chem. Soc.*, 1972, **94**, 47–57.
36 J. J. Pignatello, *Environ. Sci. Technol.*, 1992, **26**, 944–951.
37 Z. Wang, W. Qiu, S. Y. Pang, Y. Zhou, Y. Gao, C. Guan and J. Jiang, *Chem. Eng. J.*, 2019, **371**, 842–847.
38 J. Madhavan, P. Maruthamuthu, S. Murugesan and M. Ashokkumar, *Appl. Catal., A*, 2009, 35–39.
39 I. Sires, E. Guivarch, N. Oturan and M. A. Oturan, *Chemosphere*, 2008, **72**, 592–600.
40 H. L. So, W. Chu and Y. H. Wang, *Chemosphere*, 2019, **218**, 110–118.
41 J. W. T. Spinks and R. J. Woods, *Introduction to radiation chemistry*, Wiley Press, New York, 1990.
42 L. B. Donald and O. E. John, *J. Am. Chem. Soc.*, 1956, **78**, 1125–1129.
43 A. Rastogi, S. R. Ai-Abed and D. D. Dionysiou, *Appl. Catal., B*, 2009, **85**, 171–179.
44 V. Diaz, R. Ibanez, P. Gomez, A. M. Urtiaga and I. Ortiz, *Water Res.*, 2011, **45**, 125–134.
45 J. Gaffney Vde, V. V. Cardoso, M. J. Benoliel and C. M. Almeida, *J Environ. Manag.*, 2016, **166**, 466–477.
46 Z. Zhou and J. Q. Jiang, *J. Pharm. Biomed. Anal.*, 2015, **106**, 37–45.
47 K. Zhang, Z. Luo, T. Zhang, N. Gao and Y. Ma, *BioMed Res. Int.*, 2015, **2015**, 169215.
48 D. Shahidi, A. Moheb, R. Abbas, S. Larouk, R. Roy and A. Azzouz, *J. Hazard. Mater.*, 2015, **298**, 338–350.
49 S. Wang and J. Wang, *RSC Adv.*, 2017, **7**, 48670–48677.
50 J. M. Monteagudo, A. Durán, I. San Martín and P. Carrillo, *Chem. Eng. J.*, 2019, **364**, 257–268.
51 H. Milh, B. Schoenaers, A. Stesmans, D. Cabooter and R. Dewil, *Chem. Eng. J.*, 2020, **379**, 122234.
52 M. Majewsky, D. Wagner, M. Delay, S. Brase, V. Yargeau and H. Horn, *Chem. Res. Toxicol.*, 2014, **27**, 1821–1828.